Journal of Materials Chemistry C

ROYAL SOCIETY OF CHEMISTRY

PAPER

View Article Online
View Journal | View Issue



Cite this: J. Mater. Chem. C, 2020, 8, 6749

# Non-fullerene small molecule acceptors with three-dimensional thiophene/selenophene-annulated perylene diimides for efficient organic solar cells†

Jiawei Pan,[a] Ling Wang,[a] Wei Chen,[a] Shenglong Sang,[a] Hua Sun,[a] Bo Wu,[a] Xiao-Chun Hang,[a] Zhengyi Sun *[a] and Wei Huang [ab]

Received 18th January 2020,
Accepted 30th March 2020

DOI: 10.1039/d0tc00341g

rsc.li/materials-c

New three-dimensional non-fullerene small molecule acceptors were synthesized with the structure of a spiro core, 4,4′-spirobi[cyclopenta[2,1-*b*;3,4-*b*′]dithiophene] (SCPDT) linked with S/Se fused perylene diimides (PDIs). The three-dimensional structure suppresses the aggregation of PDIs and the formation of excessively large crystalline domains. The well-conjugated structure and electron-rich property of the spiro core give rise to high electron mobility, making for more balanced carrier transport. The introduction of S/Se aromatic rings leads to appropriate energy levels and more twisted molecular configurations. Organic solar cells based on the PBDB-T-S:SCPDT-PDI$_4$-S bulk heterojunction exhibit a high power conversion efficiency of 6.95% along with a high $V_{oc}$ of 1.00 V, a $J_{sc}$ of 11.72 mA cm$^{-2}$ and a fill factor of 59.27%.



## Introduction

In past decades, bulk heterojunction (BHJ) organic solar cells (OSCs) have attracted extensive attention owing to their attractive characteristics, for instance, low cost, flexibility in their fabrication, large-area printing production and environmentally friendly nature.[1–9] Polymer materials as donors and fullerene or non-fullerene materials as acceptors make up the active layers of the OSCs. Fullerene derivatives such as PC$_{61}$BM ([6,6]-phenyl-C$_{61}$-butyric acid methyl ester) and PC$_{71}$BM ([6,6]-phenyl-C$_{71}$-butyric acid methyl ester) have undergone remarkable development in the last few years and power conversion efficiencies (PCEs) of fullerene-based BHJ OSCs of over 11% have been reported.[10–12] Despite fullerene derivatives playing a significant role in the development of OSCs, their weaknesses are obvious, for example the fabrication of fullerene is costly and energy level tuning is not easy.[13,14] Hence, non-fullerene acceptors have been paid much attention in the development of OSCs. Compared with fullerene, non-fullerene acceptors have advantageous characteristics, such as tunable energy levels, appropriate optical absorption, good chemical stability and excellent morphology stability.[15–18] To date, a series of high-performance non-fullerene acceptors have been intensively developed and studied, such as perylene diimide (PDI),[19] ITIC,[14] Y6[20] and their derivatives.[16–28] Especially, thanks to their strong absorption in the near-infrared region, high electron mobility and suitable energy levels, OSCs based on Y6 or its derivative acceptors have already achieved PCEs of over 17%,[29–31] which are to date the highest efficiencies for single-junction OSCs. Meanwhile, PDI-based acceptors have also been subject to much exploration, owing to their fascinating properties such as easy accessibility, intense absorption in the visible region, high electron affinity and mobility, and excellent photochemical stability.[23,32–35] The PCEs of OSCs with PDI derivative acceptors have exceeded 10%.[24] However, PDI has a large planar structure and strong intermolecular π–π stacking, leading to the formation of excessively large crystalline domains, which may result in considerable phase separation in the active layer and thus limit the device performance.[35,36] So as to suppress the tendency to aggregate, many methods have been explored, such as the construction of twisted PDI dimers and three-dimensional structured oligomers. In addition, S,[37–39] Se[17,22] and N[40] heteroatoms have been incorporated at the bay positions of PDI units to gain more twisted structures and higher lowest unoccupied molecular orbital (LUMO) levels. Although great progress has been made in acceptors based on multidimensional PDIs, most of the previous work has focused on the structure of twisted PDI dimers. In comparison, besides suppressing the aggregation, these three-dimensional structures can further promote

[a] Key Laboratory of Flexible Electronics (KLOFE), Institute of Advanced Materials (IAM), Nanjing Tech University, 30 South Puzhu Road, Nanjing, 211816, China. E-mail: iamzysun@njtech.edu.cn
[b] Shaanxi Institute of Flexible Electronics (SIFE), Northwestern Polytechnical University, 127 West Youyi Road, Xi'an 710072, China

† Electronic supplementary information (ESI) available. See DOI: 10.1039/d0tc00341g

isotropic charge transport, which is favorable to the device performance. Therefore, it is pertinent to make high performance PDI-based acceptors by adopting the three-dimensional structures.

In this study, we report two new propeller-shaped small molecule acceptors (SMAs) named SCPDT-PDI$_4$-S and SCPDT-PDI$_4$-Se, based on a spiro core 4,4′-spirobi[cyclopenta[2,1-*b*;3,4-*b*′]dithiophene] (SCPDT) linked with S/Se fused PDIs. The spiro core SCPDT possesses an orthogonal molecular conformation with two planar cyclopenta[2,1-*b*;3,4-*b*′]dithiophene (CPDT) units connected *via* a spiro sp$^3$ carbon, and shows unique optical and electrochemical properties due to the use of thiophene as the central aromatic system to provide the π-electron conjugation.[41,42] Owing to the well-conjugated structure and electron-rich property of two CPDTs,[43] these two SMAs are expected to possess strong intramolecular charge transfer characteristics and thus broad low-energy optical transitions and high carrier mobilities. The introduction of S/Se aromatic rings has an important effect on the energy levels and molecular configurations, as well as carrier mobilities. By using SCPDT-PDI$_4$-S as the acceptor and the polymer PBDB-T-S as the donor, the OSCs show a higher PCE of 6.95% compared with that of 4.26% for SCPDT-PDI$_4$-Se-based counterparts, which is attributed to the combined properties of appropriate energy level, balanced carrier mobility and appropriate phase separation in the active layer.

## Results and discussion

### Synthesis and characterization

The synthetic routes of the two new acceptors are illustrated in Scheme 1 and Scheme S1 (ESI†). The synthesis of PDI-S uses methods borrowed from previous literature,[37] by which PDI-S was obtained through the reaction of the compound PDI-NO$_2$ with S in *N*-methyl-2-pyrrolidone (NMP) solvent. Then, it was reacted with liquid bromine at room temperature to produce monomer PDI-S-Br. Afterwards, SCPDT-PDI$_4$-S was yielded *via* Stille coupling reaction between 4Sn-SCPDT and the compound PDI-S-Br. The synthetic route of SCPDT-PDI$_4$-Se was similar to that of SCPDT-PDI$_4$-S. The compounds were characterized by NMR spectroscopy and mass spectrometry (Fig. S5–S8, ESI†). Both SCPDT-PDI$_4$-S and SCPDT-PDI$_4$-Se show good thermal stabilities (Fig. S4, ESI†), with 5% weight loss at 368.75 °C and 370.85 °C, respectively. They show excellent solubility in common organic solvents such as chloroform and chlorobenzene, which is mainly due to their 3D molecular structure and branched alkyl side chains.

### Optical and electrochemical properties

The UV-visible absorption spectra of SCPDT-PDI$_4$-S and SCPDT-PDI$_4$-Se in solutions and thin films are illustrated in Fig. 1 and the corresponding data are summarized in Table 1. As shown in Fig. 1a, the two acceptors show similar absorption profiles in dichloromethane solution ($10^{-5}$ M), while the spectrum of SCPDT-PDI$_4$-S exhibits a slight blue shift. In the range of 400–600 nm, SCPDT-PDI$_4$-S and SCPDT-PDI$_4$-Se exhibit high absorption with the peaks at 498 and 503 nm, respectively. In Fig. 1b, it can be seen that the absorption spectra of the films are quite similar to those of the solutions, indicating a weak intermolecular aggregation of the two acceptors in the solid state. The optical bandgaps ($E_g^{opt}$) of SCPDT-PDI$_4$-S and SCPDT-PDI$_4$-Se are estimated to be 1.87 and 1.84 eV, respectively, from the empirical formula $E_g^{opt} = 1240/\lambda_{onset}$. It is easy to see in Fig. 1b that the combination of the absorbances of donor molecule PBDB-T-S and these two acceptors covers the visible spectrum well. And in comparison, owing to the blue shift, the spectrum of SCPDT-PDI$_4$-S is expected to make a better combination with that of the PBDB-T-S donor. To further verify these, the absorption spectra of SCPDT-PDI$_4$-S and SCPDT-PDI$_4$-Se blended with PBDB-T-S (1 : 1, w/w) are characterized, which confirm a full harvest of light in the visible spectrum, as shown in Fig. S1 (ESI†). As expected, the PBDB-T-S:SCPDT-PDI$_4$-S blend shows superior absorbance compared with PBDB-T-S:SCPDT-PDI$_4$-Se one.

Cyclic voltammogram (CV) measurements were carried out in dichloromethane solution (Fig. S2, ESI†). The LUMO and highest occupied molecular orbital (HOMO) levels were estimated to be −3.75/−5.62 eV and −3.74/−5.58 eV for SCPDT-PDI$_4$-S and SCPDT-PDI$_4$-Se, respectively, according to the reduction onset potential and optical bandgap ($E_g^{opt}$) (Table 1). The LUMO levels of SCPDT-PDI$_4$-S and SCPDT-PDI$_4$-Se are almost the same and show a rise in comparison with that of SCPDT-PDI$_4$ (−3.80 eV),[42] which can be attributed to the introduction of S/Se aromatic ring with electron-donating ability.[17,39] The energy offset between LUMO of SCPDT-PDI-S (−3.75 eV) and HOMO of

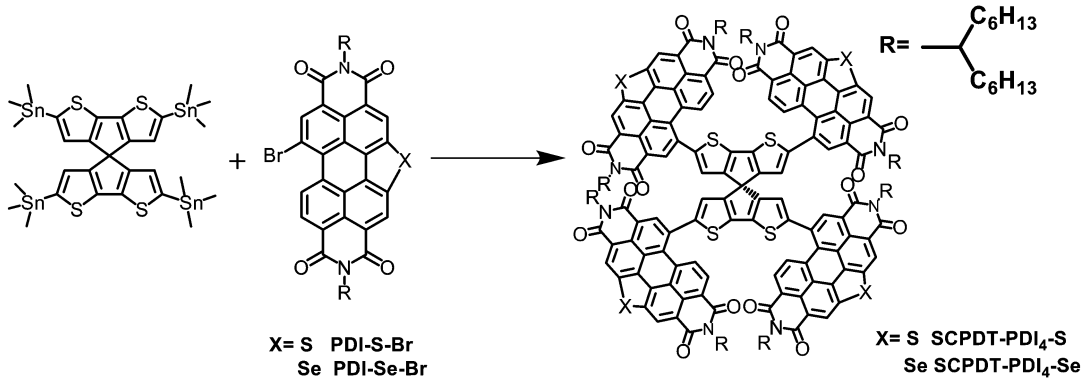


Scheme 1 Synthesis routes of SCPDT-PDI$_4$-S and SCPDT-PDI$_4$-Se.

 

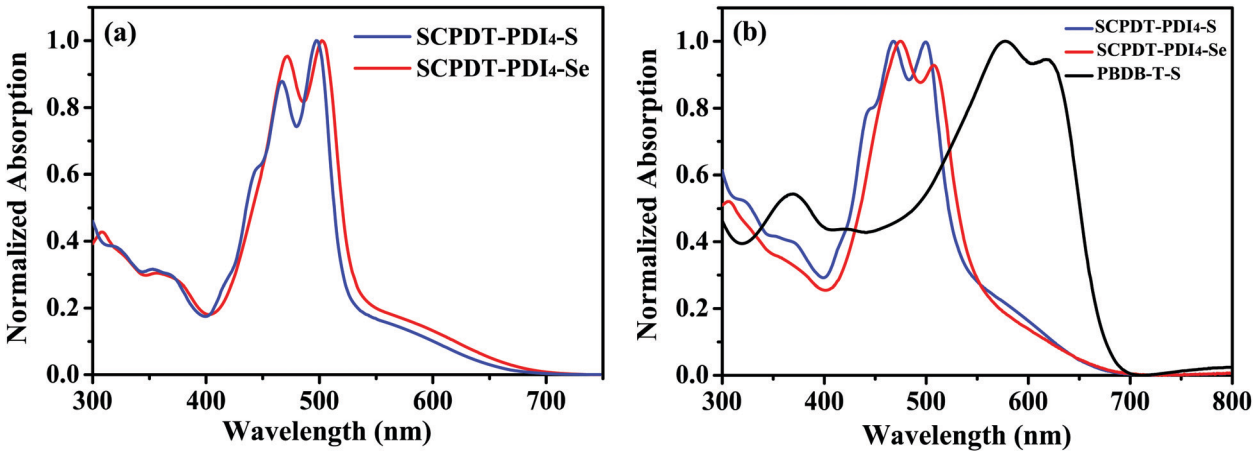


Fig. 1 (a) The normalized UV-vis absorption spectra of SCPDT-PDI$_4$-S and SCPDT-PDI$_4$-Se in dichloromethane solution ($10^{-5}$ M). (b) The normalized absorption spectra of SCPDT-PDI$_4$-S, SCPDT-PDI$_4$-Se and PBDB-T-S thin films.

Table 1 Basic properties of SCPDT-PDI$_4$-S and SCPDT-PDI$_4$-Se

| Acceptor | $\lambda_{max}$ (nm) | $\lambda_{onset}$ (nm) | $E_g^{opt}$ (eV) | HOMO (eV) | LUMO (eV) |
|---|---|---|---|---|---|
| SCPDT-PDI$_4$-S | 499 | 663 | 1.87 | −5.62 | −3.75 |
| SCPDT-PDI$_4$-Se | 509 | 674 | 1.84 | −5.58 | −3.74 |

PBDB-T-S (−5.35 eV) is 1.6 eV; therefore a high $V_{oc}$ can be reasonably expected.

### Theoretical analysis

In order to get the optimal 3D molecular geometries, density functional theory (DFT) calculations were performed at the B3LYP/6-31G(d) level.[44] For convenience of calculation, we used methyl to replace long branched alkyl chains. Both SCPDT-PDI$_4$-S and SCPDT-PDI$_4$-Se show 3D nonplanar configurations, which should contribute to suppressing aggregation tendency and intermolecular stacking. As shown in Fig. 2, the LUMOs of SCPDT-PDI$_4$-S and SCPDT-PDI$_4$-Se are mainly located on the SCPDT core, while the HOMOs are distributed on peripheral PDIs, which implies a polarization in the excited state. The LUMO/HOMO levels of SCPDT-PDI$_4$-S and SCPDT-PDI$_4$-Se are −3.52/−5.77 eV and −3.49/−5.77 eV, respectively, from DFT calculations, which are consistent with the experimental values from the CV measurements. Moreover, the four dihedral angles between CPDT and the PDI unit are 81.88°, 77.10°, 78.07° and 80.07° for SCPDT-PDI$_4$-S, and 81.20°, 74.26°, 74.42° and 80.97° for SCPDT-PDI$_4$-Se (see Fig. 2). Compared with the value of 59°

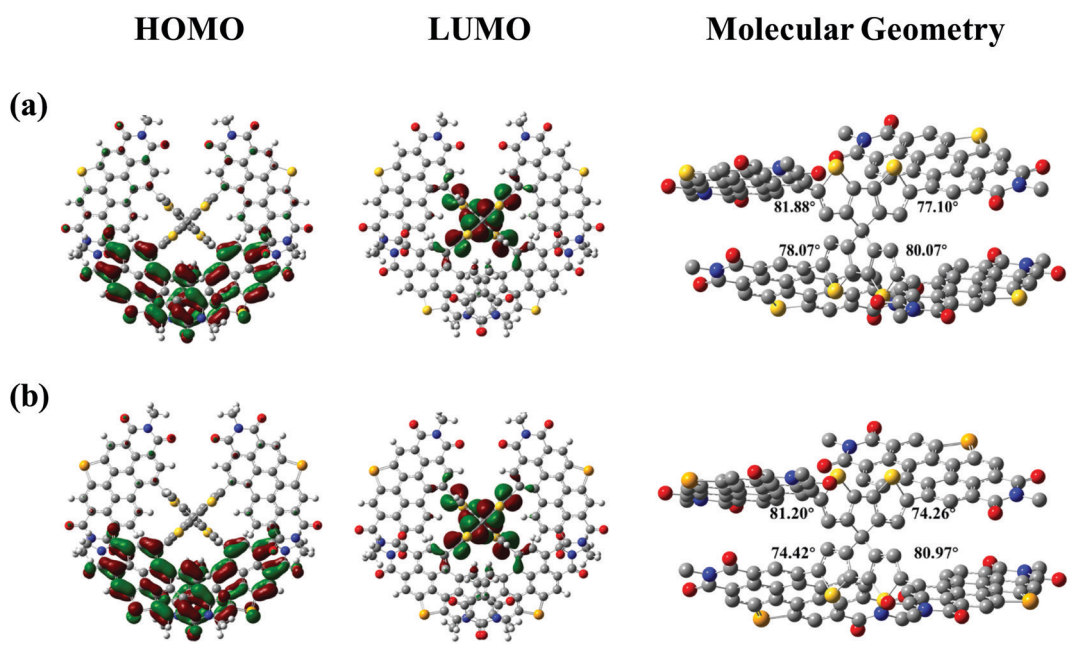


Fig. 2 HOMOs, LUMOs and optimized molecular geometries of (a) SCPDT-PDI$_4$-S and (b) SCPDT-PDI$_4$-Se calculated by DFT at the B3LYP/6-31G(d) level.

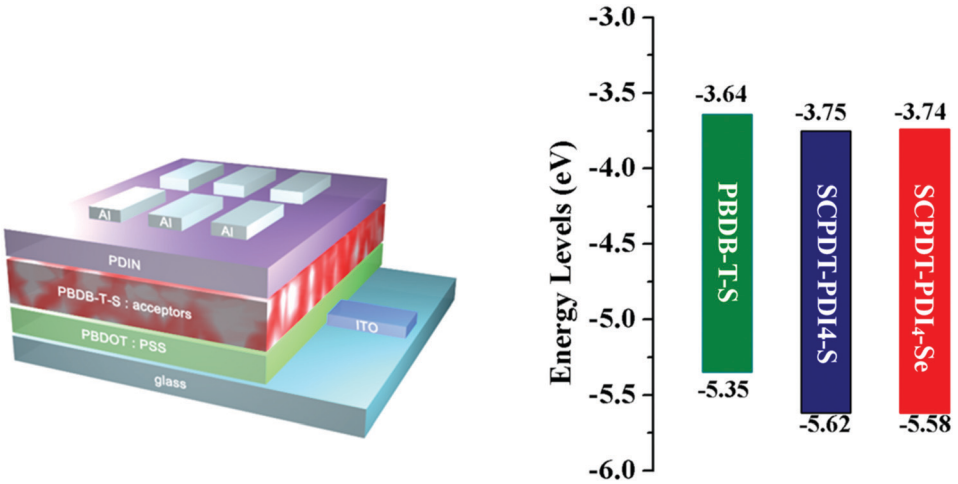


Fig. 3 Device configuration of the OSCs and energy levels of PBDB-T-S, SCPDT-$PDI_4$-S and SCPDI-$PDI_4$-Se.

for all these dihedral angles in SCPDT-$PDI_4$,[34] this remarkable increase clearly indicates that the introduction of an S/Se aromatic ring (especially thiophene) leads to a more twisted molecular structure, which is beneficial to the suppression of molecular aggregation and the blending of donor and acceptor in the active layer.

### Photovoltaic properties

OSCs using SCPDT-$PDI_4$-S and SCPDT-$PDI_4$-Se as acceptors were fabricated with the conventional architecture of ITO/poly(3,4-ethylenedioxythiophene):poly(styrenesulfonate) (PEDOT:PSS)/PBDB-T-S:acceptors/2,9-bis[(3-(dimethylamino)propyl)anthra[2,1,9-*def*:6,5,10-*def*']diisoquinoline-1,3,8,10(2*H*,9*H*)-tetraone) (PDIN)/Al, as shown in Fig. 3 and Fig. S3 (ESI†). The wide bandgap polymer PBDB-T-S was selected as the donor owing to its complementary absorbance and matched energy levels with SCPDT-$PDI_4$-S and SCPDT-$PDI_4$-Se. In our experiment, the optimal donor–acceptor weight ratio was found to be 1 : 1, with a total concentration of 20 mg $mL^{-1}$ in dichlorobenzene. The current density–voltage (*J*–*V*) characteristics of the devices are shown in Fig. 4a and the parameters are summarized in Table 2. The PBDB-T-S:SCPDT-$PDI_4$-S-based device (SCPDT-$PDI_4$-S device) achieves a high PCE of 6.95% along with a high $V_{oc}$ of 1.00 V, $J_{sc}$ of 11.72 mA $cm^{-2}$ and fill factor (FF) of 59.27%, while the PBDB-T-S:SCPDT-$PDI_4$-Se-based device (SCPDT-$PDI_4$-Se device) has a PCE of 4.26%, along with a $V_{oc}$ of 0.97 V, $J_{sc}$ of 8.70 mA $cm^{-2}$ and FF of 50.55%. It can be easily seen the SCPDT-$PDI_4$-S device shows the much higher $J_{sc}$, which can be ascribed to the more complementary absorbance of SCPDT-$PDI_4$-S with the donor molecule. In addition, the larger FF of the SCPDT-$PDI_4$-S device is believed to arise from the more favorable morphology of PBDB-T-S:SCPDT-$PDI_4$-S film compared with that of PBDB-T-S:SCPDT-$PDI_4$-Se film, which would reduce the impedance at the interface. Note that the SCPDT-$PDI_4$-S device also shows a higher efficiency than the SCPDT-$PDI_4$-based device with the different polymer donor PTB7-Th (PCE = 6.31%, without additive), as reported in the literature.[42] In our study, the donor PTB7-Th paired with SCPDT-$PDI_4$-S and SCPDT-$PDI_4$-Se acceptors was also tried but led to a relatively low performance.

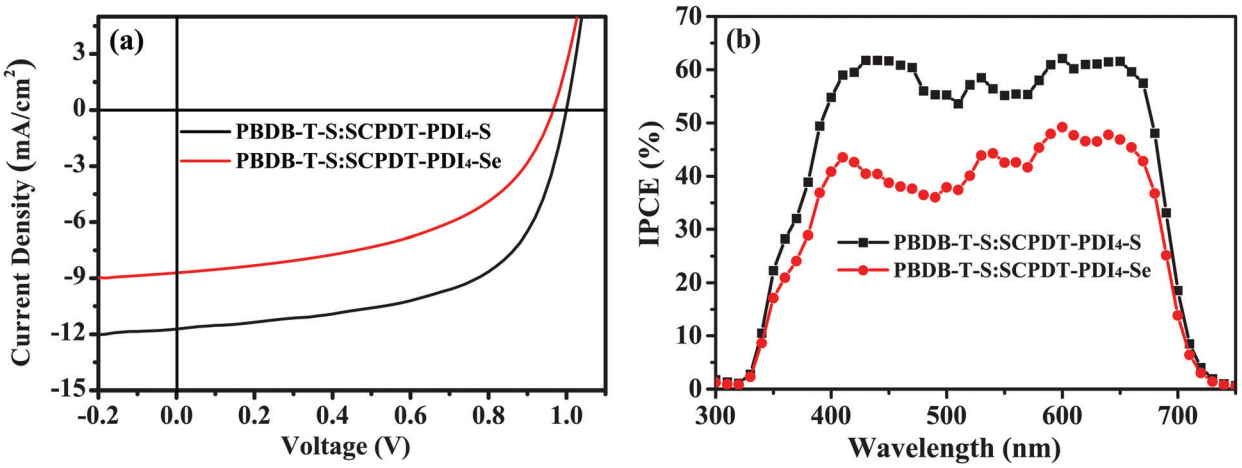


Fig. 4 (a) *J*–*V* curves and (b) IPCE spectra of the OSCs with PBDB-T-S:SCPDT-$PDI_4$-S and PBDB-T-S:SCPDT-$PDI_4$-Se absorber layers under illumination of AM 1.5G at 100 mW $cm^{-2}$.

Table 2 Performance of the optimized OSC devices based on the active layer of PBDB-T-S:acceptor (1 : 1, w/w) under illumination of AM 1.5G at 100 mW $cm^{-2}$

| Active layer | $V_{oc}$ (V) | $J_{sc}$ (mA) | FF (%) | PCE[a] (%) | $\mu_h$ ($cm^2$ $V^{-1}$ $s^{-1}$) | $\mu_e$ ($cm^2$ $V^{-1}$ $s^{-1}$) | $\mu_h/\mu_e$ |
|---|---|---|---|---|---|---|---|
| PBDB-T-S:SCPDT-$PDI_4$-S | 1.00 | 11.72 | 59.27 | 6.95 (6.90) | $1.960 \times 10^{-5}$ | $1.751 \times 10^{-5}$ | 1.12 |
| PBDB-T-S:SCPDT-$PDI_4$-Se | 0.97 | 8.70 | 50.55 | 4.26 (4.16) | $1.779 \times 10^{-5}$ | $1.097 \times 10^{-5}$ | 1.62 |

[a] The first value in each is the best PCE, while the one in parentheses is the average PCE collected from 10 independent devices.

The incident photon to current efficiency (IPCE) spectra of the SCPDT-$PDI_4$-S device and SCPDT-$PDI_4$-Se device are displayed in Fig. 4b. Both the PBDB-T-S:SCPDT-$PDI_4$-S and PBDB-T-S:SCPDT-$PDI_4$-Se blend films exhibit a broad spectral response from 320 to 720 nm. The optimal SCPDT-$PDI_4$-S device exhibits a stronger photo response in the wavelength range of 400–670 nm with a maximum quantum efficiency of 62%. The $J_{sc}$ values integrated from the IPCE data are 11.34 and 8.33 mA $cm^{-2}$ for the SCPDT-$PDI_4$-S and SCPDT-$PDI_4$-Se devices, respectively, which are consistent with the values obtained from the *J–V* measurements (less than 5% mismatch).

To further account for the superior performance of the SCPDT-$PDI_4$-S device, the morphologies and the charge carrier mobilities of the OSC active layers were investigated. The surface morphology was characterized by atomic force microscopy (AFM) and transmission electron microscopy (TEM). It can be seen in Fig. 5a–d that the as-cast blend films of PBDB-T-S:SCPDT-$PDI_4$-S and PBDB-T-S:SCPDT-$PDI_4$-Se display

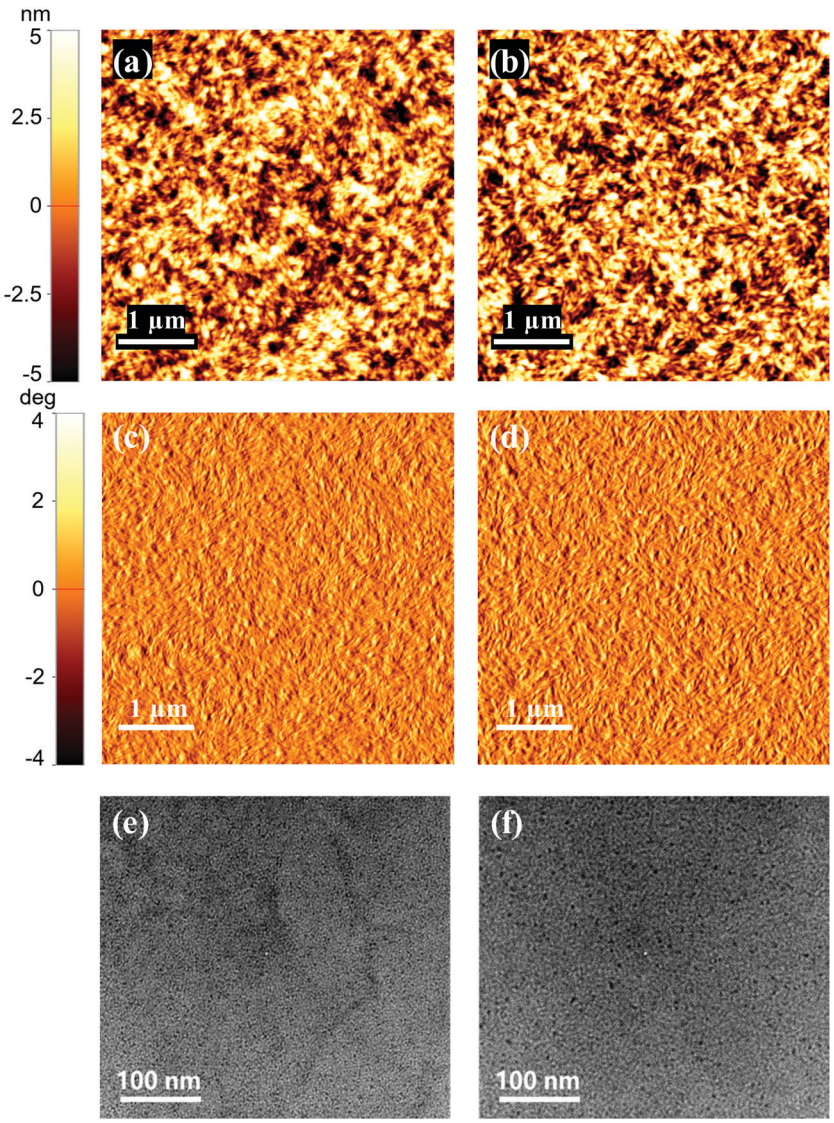


Fig. 5 Morphology images of PBDB-T-S:SCPDT-$PDI_4$-S (1 : 1, w/w; left) and PBDB-T-S:SCPDT-$PDI_4$-Se (1 : 1, w/w; right) blend films: (a) and (b), AFM height; (c) and (d), AFM phase; (e) and (f), TEM images.

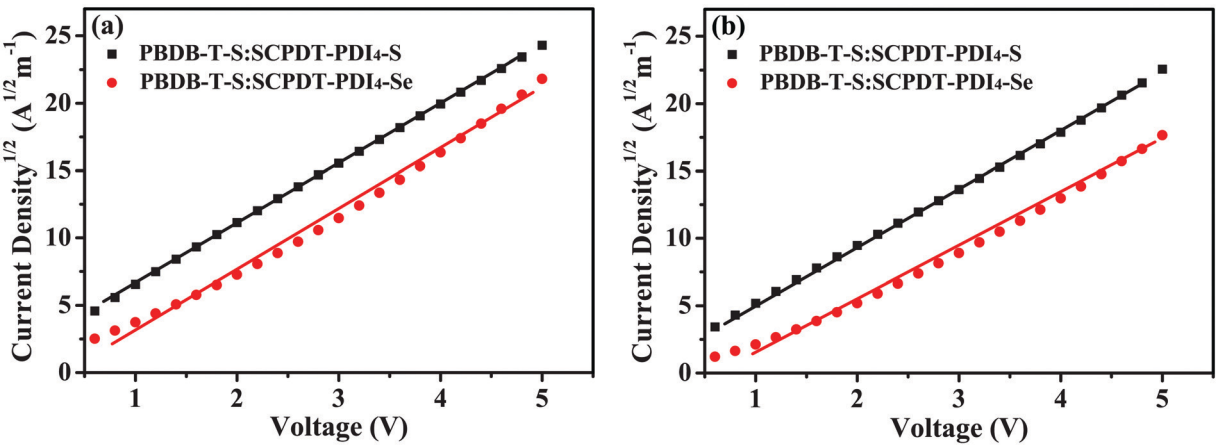


Fig. 6 Dark current density–voltage characteristics for (a) hole-only devices and (b) electron-only devices with optimized PBDB-T-S:SCPDT-PDI$_4$-S and PBDB-T-S:SCPDT-PDI$_4$-Se active layers.

smooth and uniform morphologies. The root mean square (RMS) surface roughness values are 2.443 nm and 2.705 nm, respectively. No distinct molecular aggregations between the donor PBDB-T-S and the two acceptors take place. Compared with the PBDB-T-S:SCPDT-PDI$_4$-Se film, the PBDB-T-S:SCPDT-PDI$_4$-S film exhibits some improvement in the RMS surface roughness values, which could be beneficial to the enhancement of FF and $J_{sc}$ in the device.[23] The AFM image of the PBDB-T-S:SCPDT-PDI$_4$-S film also seems to exhibit a certain nanofibrillar structure, which facilitates charge collection and transport. The TEM images demonstrate that the domain size of the PBDB-T-S:SCPDT-PDI$_4$-S film is smaller than that of the PBDB-T-S:SCPDT-PDI$_4$-Se film (Fig. 5e and f), indicating more suppressed aggregation, which will facilitate exciton dissociation and hence improve the FF and $J_{sc}$. As expected, SCPDT-PDI$_4$-S, with the more twisted molecular configuration, gives rise to better surface morphology of the blend film.

Charge transport characteristics play an important role in device performance; hence we investigated the charge carrier mobility of the donor–acceptor blend film with the space-charge-limited current (SCLC) method, as shown in Fig. 6. Hole-only and electron-only devices were fabricated with the structures ITO/PETDOT:PSS/active layer/$MoO_3$/Al and ITO/ZnO/active layer/PDIN/Al, respectively. The hole mobilities ($\mu_h$) of PBDB-T-S:SCPDT-PDI$_4$-S and PBDB-T-S:SCPDT-PDI$_4$-Se active layers were calculated to be $1.960 \times 10^{-5}$ and $1.779 \times 10^{-5}$ cm$^2$ V$^{-1}$ s$^{-1}$, respectively, while the electron mobilities ($\mu_e$) are $1.751 \times 10^{-5}$ and $1.097 \times 10^{-5}$ cm$^2$ V$^{-1}$ s$^{-1}$, respectively. Therefore, PBDB-T-S:SCPDT-PDI$_4$-S shows higher $\mu_h$ and $\mu_e$ values as well as more balanced $\mu_h/\mu_e$ values compared with PBDB-T-S:SCPDT-PDI$_4$-Se (see Table 2), which also reasonably accounts for the higher $J_{sc}$ and FF values of SCPDT-PDI$_4$-S device.

## Conclusions

In summary, we designed and synthesized two new non-fullerene SMAs of SCPDT-PDI$_4$-S and SCPDT-PDI$_4$-Se with SCPDT as the spiro core and PDI-S and PDI-Se as the peripheral groups. In comparison with SCPDT-PDI$_4$-Se, SCPDT-PDI$_4$-S exhibits the more suitable absorption properties and more twisted molecular configuration, as well as higher carrier mobility in the blend film. The BHJ OSCs based on the PBDB-T-S:SCPDT-PDI$_4$-S active layer achieve a high PCE of 6.95%, with $V_{oc}$ of 1.00 V, $J_{sc}$ of 11.72 mA cm$^{-2}$ and FF of 59.27%, showing a better performance than PTB7-Th:SCPDT-PDI$_4$-based devices without additive, while the OSCs based on the PBDB-T-S:SCPDT-PDI$_4$-Se active layer show lower performance. The good photovoltaic property of SCPDT-PDI$_4$-S makes it a suitable candidate for non-fullerene acceptors in OSCs. The design strategy of SMAs with suitable spiro core and S-annulated PDI end groups is a simple and efficient method to achieve high performance OSCs. It can be expected that with further optimization of energy levels and optical absorption, the corresponding devices can achieve better efficiency in the future.

## Conflicts of interest

There are no conflicts of interest to declare.

## Acknowledgements

We gratefully acknowledge financial support from the Natural Science Foundation of Jiangsu Province (Grant No. BK20191358, BK20181373 and BK20170985) and the National Natural Science Foundation of China (Grant No. 11504168). We are also grateful to the High Performance Computing Center of Nanjing Tech University for the supporting computational resources.

## Notes and references

1 J. Hou, O. Inganäs, R. H. Friend and F. Gao, *Nat. Mater.*, 2018, **17**, 119.
2 G. Li, W.-H. Chang and Y. Yang, *Nat. Rev. Mater.*, 2017, **2**, 17043.
3 Y. Lin and X. Zhan, *Acc. Chem. Res.*, 2015, **49**, 175.

 

4 L. Lu, M. A. Kelly, W. You and L. Yu, *Nat. Photonics*, 2015, **9**, 491.
5 C. B. Nielsen, S. Holliday, H.-Y. Chen, S. J. Cryer and I. McCulloch, *Acc. Chem. Res.*, 2015, **48**, 2803.
6 P. Sonar, J. P. F. Lim and K. L. Chan, *Energy Environ. Sci.*, 2011, **4**, 1558.
7 V. Vohra, K. Kawashima, T. Kakara, T. Koganezawa, I. Osaka, K. Takimiya and H. Murata, *Nat. Photonics*, 2015, **9**, 403.
8 C. Yan, S. Barlow, Z. Wang, H. Yan, A. K.-Y. Jen, S. R. Marder and X. Zhan, *Nat. Rev.*, 2018, **3**, 18003.
9 G. Zhang, J. Zhao, P. C. Chow, K. Jiang, J. Zhang, Z. Zhu, J. Zhang, F. Huang and H. Yan, *Chem. Rev.*, 2018, **118**, 3447.
10 Z. He, B. Xiao, F. Liu, H. Wu, Y. Yang, S. Xiao, C. Wang, T. P. Russell and Y. Cao, *Nat. Photonics*, 2015, **9**, 174.
11 L. Lu, T. Zheng, Q. Wu, A. M. Schneider, D. Zhao and L. Yu, *Chem. Rev.*, 2015, **115**, 12666.
12 J. Zhao, Y. Li, G. Yang, K. Jiang, H. Lin, H. Ade, W. Ma and H. Yan, *Nat. Energy*, 2016, **1**, 15027.
13 S. Holliday, R. S. Ashraf, C. B. Nielsen, M. Kirkus, J. A. Röhr, C.-H. Tan, E. C. Fregoso, A. C. Knall, J. R. Durrant, J. Nelson and I. McCulloch, *J. Am. Chem. Soc.*, 2015, **137**, 898.
14 Y. Lin, J. Wang, Z.-G. Zhang, H. Bai, Y. Li, D. Zhu and X. Zhan, *Adv. Mater.*, 2015, **27**, 1170.
15 Z. Luo, H. Bin, T. Liu, Z.-G. Zhang, Y. Yang, C. Zhong, B. Qiu, G. Li, W. Gao, D. Xie, K. Wu, Y. Sun, F. Liu, Y. Li and C. Yang, *Adv. Mater.*, 2018, **30**, 1706124.
16 J. Liu, S. Chen, D. Qian, B. Gautam, G. Yang, J. Zhao, J. Bergqvist, F. Zhang, W. Ma, H. Ade, O. Inganäs, K. Gundogdu, F. Gao and H. Yan, *Nat. Energy*, 2016, **1**, 16089.
17 D. Meng, D. Sun, C. Zhong, T. Liu, B. Fan, L. Huo, Y. Li, W. Jiang, H. Choi, T. Kim, J. Y. Kim, Y. Sun, Z. Wang and A. J. Heeger, *J. Am. Chem. Soc.*, 2015, **138**, 375.
18 Y. Zhong, M. T. Trinh, R. Chen, G. E. Purdum, P. P. Khlyabich, M. Sezen, S. Oh, H. Zhu, B. Fowler, B. Zhang, W. Wang, C. Nam, M. Y. Sfeir, C. T. Black, M. L. Steigerwald, Y. Loo, F. Ng, X. Zhu and C. Nuckolls, *Nat. Commun.*, 2015, **6**, 8242.
19 X. Zhan, A. Facchetti, S. Barlow, T. J. Marks, M. A. Ratner, M. R. Wasielewski and S. R. Marder, *Adv. Mater.*, 2011, **23**, 268.
20 J. Yuan, Y. Zhang, L. Zhou, G. Zhang, H.-L. Yip, T.-K. Lau, X. Lu, C. Zhu, H. Peng, P. A. Johnson, M. Leclerc, Y. Cao, J. Ulanski, Y. Li and Y. Zou, *Joule*, 2019, **3**, 1140.
21 S. Li, L. Ye, W. Zhao, S. Zhang, S. Mukherjee, H. Ade and J. Hou, *Adv. Mater.*, 2016, **28**, 9423.
22 Z. Luo, T. Liu, Z. Chen, Y. Xiao, G. Zhang, L. Huo, C. Zhong, X. Lu, H. Yan, Y. Sun and C. Yang, *Adv. Sci.*, 2019, **6**, 1802065.
23 D. Meng, H. Fu, C. Xiao, X. Meng, T. Winands, W. Ma, W. Wei, B. Fan, L. Huo, N. L. Doltsinis, Y. Li, Y. Sun and Z. Wang, *J. Am. Chem. Soc.*, 2016, **138**, 10184.
24 J. Zhang, Y. Li, J. Huang, H. Hu, G. Zhang, T. Ma, P. C. Chow, H. Ade, D. Pan and H. Yan, *J. Am. Chem. Soc.*, 2017, **139**, 16092.
25 F. Zhao, S. Dai, Y. Wu, Q. Zhang, J. Wang, L. Jiang, Q. Ling, Z. Wei, W. Ma, W. You, C. Wang and X. Zhan, *Adv. Mater.*, 2017, **29**, 1700144.
26 B. Fan, D. Zhang, M. Li, W. Zhong, Z. Zeng, L. Ying, F. Huang and Y. Cao, *Sci. China: Chem.*, 2019, **62**, 746.
27 Y. Cui, H. Yao, J. Zhang, T. Zhang, Y. Wang, L. Hong, K. Xian, B. Xu, S. Zhang, J. Peng, Z. Wei, F. Gao and J. Hou, *Nat. Commun.*, 2019, **10**, 2515.
28 G. Li, S. Wang, T. Liu, P. Hao, Z. Liu, F. Li, L.-M. Yang, Y. Zhang, D. Li, S. Yang, J. Zhao, J. Li, H. Yan and B. Tang, *J. Mater. Chem. C*, 2018, **6**, 12601.
29 Y. Lin, B. Adilbekova, Y. Firdaus, E. Yengel, H. Faber, M. Sajjad, X. Zheng, E. Yarali, A. Seitkhan, O. M. Bakr, A. El-Labban, U. Schwingenschlögl, V. Tung, I. McCulloch, F. Laquai and T. D. Anthopoulos, *Adv. Mater.*, 2019, **31**, 1902965.
30 Y. Lin, Y. Firdaus, M. I. Nugraha, F. Liu, S. Karuthedath, A.-H. Emwas, W. Zhang, A. Seitkhan, M. Neophytou, H. Faber, E. Yengel, I. McCulloch, L. Tsetseris, F. Laquai and T. D. Anthopoulos, *Adv. Sci.*, 2020, 1903419.
31 L. Zhan, S. Li, T. Lau, Y. Cui, X. Lu, M. Shi, C. Li, H. Li, J. Hou and H. Chen, *Energy Environ. Sci.*, 2020, **13**, 635.
32 Y. Duan, X. Xu, H. Yan, W. Wu, Z. Li and Q. Peng, *Adv. Mater.*, 2017, **29**, 1605115.
33 T. Liu, D. Meng, Y. Cai, X. Sun, Y. Li, L. Huo, F. Liu, Z. Wang, T. P. Russell and Y. Sun, *Adv. Sci.*, 2016, **3**, 1600117.
34 H. Sun, X. Song, J. Xie, P. Sun, P. Gu, C. Liu, F. Chen, Q. Zhang, Z.-K. Chen and W. Huang, *ACS Appl. Mater. Interfaces*, 2017, **9**, 29924.
35 Z. Liu, Y. Wu, Q. Zhang and X. Gao, *J. Mater. Chem. A*, 2016, **4**, 17604.
36 Y. Lin and X. Zhan, *Adv. Energy Mater.*, 2015, **5**, 1501063.
37 W. Fan, N. Liang, D. Meng, J. Feng, Y. Li, J. Hou and Z. Wang, *Chem. Commun.*, 2016, **52**, 11500.
38 Z. Luo, T. Liu, W. Cheng, K. Wu, D. Xie, L. Huo, Y. Sun and C. Yang, *J. Mater. Chem. C*, 2018, **6**, 1136.
39 D. Sun, D. Meng, Y. Cai, B. Fan, Y. Li, W. Jiang, L. Huo, Y. Sun and Z. Wang, *J. Am. Chem. Soc.*, 2015, **137**, 11156.
40 J. Cann, S. Dayneko, J.-P. Sun, A. D. Hendsbee, I. G. Hill and G. C. Welch, *J. Mater. Chem. C*, 2017, **5**, 2074.
41 J. Londenberg, T. P. Saragi, I. Suske and J. Salbeck, *Adv. Mater.*, 2007, **19**, 4049.
42 H. Sun, P. Sun, C. Zhang, Y. Yang, X. Gao, F. Chen, Z. Xu, Z.-K. Chen and W. Huang, *Chem. – Asian J.*, 2017, **12**, 721.
43 M. Wang, H. Wang, T. Yokoyama, X. Liu, Y. Huang, Y. Zhang, T.-Q. Nguyen, S. Aramaki and G. C. Bazan, *J. Am. Chem. Soc.*, 2014, **136**, 12576.
44 J. W. Ponder, *TINKER: Software Tools for Molecular Design*, Washington University School of Medicine, Saint Louis, MO, 2014.